EDUCTION SCHEME FOR CONVECTIVE STRUCTURES IN TURBULENT COMPRESSIBLE SEPARATED FLOW

Tetyana Jiang
IUSTI, Aix - Marseille Université and
UMR CNRS 7343
5 rue Enrico Fermi, 13453
Marseille Cedex 13, France
jiangt@polytech.univ-mrs.fr

Lionel Larchevêque
IUSTI, Aix - Marseille Université and
UMR CNRS 7343
5 rue Enrico Fermi, 13453
Marseille Cedex 13, France
lionel.larcheveque@polytech.univ-mrs.fr

Pierre Dupont
IUSTI, Aix-Marseille Université, UMR CNRS 7343
5 rue Enrico Fermi, 13453 Marseille Cedex 13, France
pierre.dupont@polytech.univ-mrs.fr

ABSTRACT

Evidence of coherent convective vortical structures in a statistical sense is obtained for a turbulent compressible separated flow. Structures are detected and tracked in unsteady data from a Large Eddy Simulations of shock wave-boundary layer interaction by means of a new algorithm. This one is based on the detection of the modulations of the instantaneous zero mass flux lines induced by the travelling structures. The educed structures are spatially characterized and their frequencies, convection velocities and dimensions are given. Their effect on the wall pressure and the skin friction coefficients are also described.

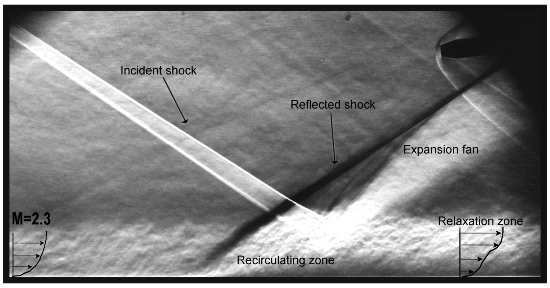

Figure 1. Spark Schlieren visualization of the interaction.

INTRODUCTION

Shock-wave/boundary-layer interaction (SWBLI) has been largely studied for several decades due to their practical interest in aeronautical applications. One critical feature of such flows is the occurrence of low-frequency unsteadiness if the shock-induced adverse pressure gradient is strong enough to induce a separation of the incoming boundary layer. The physics resulting in these low-frequency unsteadiness, also encountered in many subsonic separated flow (Cherry *et al.*, 1984; Kiya & Sasaki, 1983) is not yet fully understood, see Babinsky & Harvey (2011). However, possible links between the low-frequency unsteadiness and the coherent structures of the mixing layer developing downstream the separation point have been highlighted in recent works, both in subonic (Ehrenstein & Gallaire, 2008) and supersonic regime (Piponniau *et al.*, 2009). It is therefore of importance to obtain a comprehensive description of the characteristics of these structures. Difficulty arise in turbulent flows from the energy preeminence of the structures issued from the incoming boundary layer over the mixing layer ones. Some information where nonetheless obtained in SWBLI from two-point statistics and instantaneous PIV measurements of Dupont *et al.* (2006); Piponniau *et al.* (2009). The purpose of the present work is to complete these data by providing a statistical description of the dynamics associated with these structures. A conditional averaging method relying on a new eduction scheme of the coherent structures is proposed to this end. As an illustration, it is applied to data obtained from a Large-Eddy Simulation of a Mach 2.3 shock reflection for flow deflection angle of 9.5° including a large separation, as described in Agostini *et al.* (2012). The unsteady properties have been widely validated against the experimental results obtained for the same interaction geometry Agostini *et al.* (2012). The spatial organization of the flow is illustrated with a short time exposure Schlieren of the interaction in figure 1. The origin of the longitudinal coordinate x was fixed at the mean position (X_0) of the unsteady reflected shock. This position was derived from unsteady wall pressure. It was normalized by the length of interaction L defined as the distance between X_0 and the extrapolation down to the wall of the incident shock. The size of the interaction was of 54.5 mm. The dimensionless longitudinal coordinate $X^* = (x - X_0)/L$ was used to present the results.

One key feature of this database is the very long physical time of 150 periods of the low frequency phenomenon that has been computed. It therefore ensure a rather good statistical convergence of the conditionally averaged data.

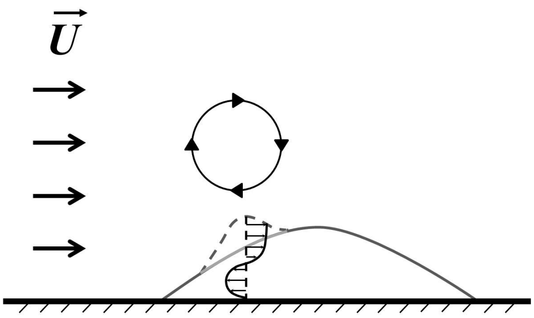

Figure 2. Sketch of the instantaneous deformation (dashed line) of the mean zero mass flux line (solid line) induced by a vortical structure from the mixing layer.

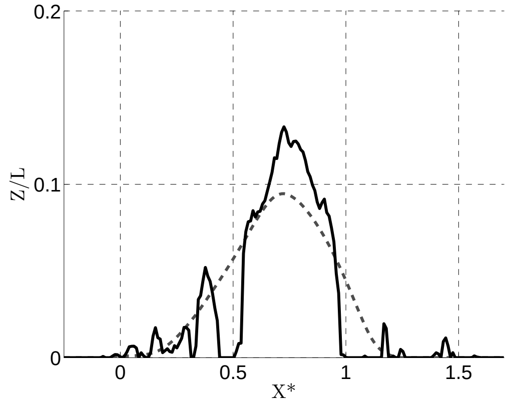

Figure 3. Averaged zero mass flux line $h(x,t)$ (dashed line) and instantaneous zero mass flux line $\overline{h(x)}$ (solid line).

CONDITIONAL AVERAGING SCHEME
Foundation

For the SWBLI flow under consideration, both PIV measurements by Dupont *et al.* (2006) and LES computations by Agostini *et al.* (2012) have shown that the mixing layer developing over the separated region is located in the vicinity of the mean dividing streamline. Structures developing and being convected along the mixing layer can hence locally alter the instantaneous dividing surface located beneath them, as conceptually illustrated in Figure 2.

It is consequently expected that a conditional averaging based on some metrics related to the dividing stream surface will be able to put in evidence the coherent vortical structures of the shear layer in a statistical sense.

Difficulty arises from the fact that the dividing stream surface is extremely difficult to extract from unsteady three-dimensional turbulent data. One can however remark that, for a Favre averaged flow with spanwise homogeneity, the dividing streamline coincides with the line on which the mass flux, integrated from the wall, vanishes from negative values. Note that if density variations are not taken into account, the former line matches the dividing streamline in the Reynolds averaged sense. It is therefore proposed to approximate the instantaneous dividing stream surface by computing the spanwise-averaged zero mass flux line. Its elevation $h(x,t)$ is such as:

$$\int_0^{h(x,t)} \left[\int_{-W/2}^{W/2} \rho(x,y,z,t) u(x,y,z,t) dy \right] dz = 0 \qquad (1)$$

where $W = 1.6\delta$ is the width of the computational domain. Note that the use of a spanwise integration, although not mandatory, allows an extra damping of the influence of the streamwise aligned structures associated with the incoming boundary layer.

The way the instantaneous zero mass flux line could be locally distorted by vortical structures convected within the mixing layer is sketched in Figure 2. The mostly spanwise-aligned structure induces a local decrease in the streamwise velocity U beneath it, resulting in a local elevation of the instantaneous zero mass flux line $h(x,t)$ compared to the time-averaged one. Using the LES database, it has indeed been found that the instantaneous line is strongly distorted compared to the mean one. It can be checked by looking at Figure 3, where the instantaneous and mean lines are plotted in solid and dashed lines, respectively. Moreover, peaks of the instantaneous line that could be induced by vortical structures according to the model of Figure 2 mostly exhibit a convective behavior when tracked in time. Maxima of the instantaneous mass flux line consequently appear to be good candidate in order to seek for the coherent structures of the mixing layer.

Eduction algorithm

Although several maxima could be tracked in time, it has been chosen to seek for the largest structures at a given time only, in order to keep the complexity of the method as low as possible. It is proposed to associate the streamwise location of the largest structure with the streamwise location of the largest *normalized relative* elevation of the zero mass flux line $h^*(t)$, defined as follow :

$$h^*(t) = \max_x \left(\frac{h(x,t) - \overline{h(x)}}{\sigma_h^*(x)} \right) \qquad (2)$$

where $\overline{h(x)} = \frac{1}{N} \sum_j h(x,t_j)$ is the time-averaged zero mass flux line, $\sigma_h^*(x)$ is the thresholded standard deviation of $h(x,t)$ defined by $\sigma_h^*(x) = \max(\sigma_h(x), s)$. The criteria defined by Equation 2 allow to take into account :

- the steady streamwise variation of the line, that is canceled in Equation 2 by subtracting the time-averaged value $\overline{h(x)}$;
- the increase in the size of the vortical structures along the mixing layer, that is taken into account by normalizing with the standard deviation $\sigma_h(x)$;
- the prevention of false detection in region where $\sigma_h(x)$ tends toward zero by the introduction of the threshold s.

The streamwise location $x_{h^*}(t)$, defined as the location at which $h^*(t)$ is encountered, is then tracked for every timestep. A typical time evolution of $x_{h^*}(t)$ is plotted in Figure 4 where the serrated evolution of x_{h^*} with time suggests the presence of convective phenomena. Velocities that can be computed from this plot are rather dispersed but their mean value is in good agreement with two-point measurements performed in the mixing layer region by Dupont *et al.* (2006). Moreover, the plot of Figure 4 demonstrates

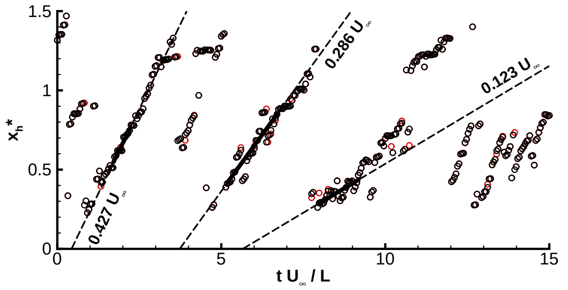

Figure 4. Time evolution of the location $x_{h^*}(t)$ at which $h^*(x,t)$ is encountered. Dashed line is the best linear fit in the least-squares sense. Black circles corresponds to results from the standard algorithm while red circles denote locations computed by removing the ρ dependence in Equation 1.

the ability of the above-described method to qualitatively track events over significant distance/time. This feature is optimized by adjusting the value of the threshold s so has to obtain a distribution of x_{h^*} as homogeneous as possible.

One may finally remark that, according to Equation 1, the density field is required to compute $x_{h^*}(t)$. This is not a constraint for the present work since the database that is used comes from a LES and therefore give access to density data. However experimental database generally do not include measurements of the density field. It is therefore of interest to note that the results described above are not significantly altered when the density is removed from Equation 1, despite the fact that the flow is fully compressible, with a convective Mach number of the mixing layer close to unity. This is demonstrated in Figure 4 on which the locations x_{h^*} obtained when ignoring the influence of the density are plotted in red.

Conditional averaging

The tracking method described in the previous section could be used to educe vortices in a time-dependant way. However it would probably suffer from a high level of misdetection because of the imperfect removal of the influence of the incoming boundary layer structures. It is rather proposed to perform a conditional averaging of the flowfield according to the location of the educed structures. The conditioning criterion is obtained by dividing the region spanned by the $x_h^*(t)$, corresponding to $X^* \in [0.166, 1.432]$, into ten intervals of equal width. The instantaneous data are then sorted into ten classes according to the interval in which $x_h^*(t)$ lies. Eventually an average over data from each class is performed, yielding conditionally averaged data. They formally correspond to a double decomposition of a variable C into a coherent part $\breve{C}_i$ and an incoherent part C_i" with ten classes $i = 1 \dots 10$. The triple decomposition can be obtained by considering the coherent fluctuation $\hat{C}_i$ defined by $\hat{C}_i = \breve{C}_i - \overline{C}$.

Before performing statistical study on the conditionally averaged data, it is of importance to check the underlying foundations of this work sketched in Figure 2. Class-averaged zero mass flux line are computed to this end. Lines for classes 2 and 9 are compared with the time-average zero mass flux line $\overline{h(x)}$ in Figure 5. The definitions of the intervals used for the conditioning algorithm are also shown on this plot. The difference between both lines is very small

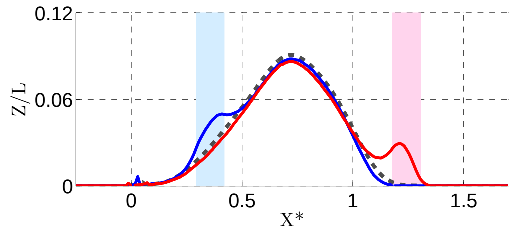

Figure 5. Class averaged zero mass flux line (solid line) and average zero mass flux line $\overline{h(x)}$ (dashed line) for classes 2 and 9 (blue and red respectively). The definition of the interval used in conditioning algorithm is also shown.

except for the intervals of X^* corresponding to each class. The localized nature of the disturbances demonstrates that the conditioning algorithm is rather insensitive to a global breathing of the separation bubble. These results confirm the idea of the spatial location of the disturbances of the zero mass flux line that is supposed to be mostly modulated by the coherent structures of the shear layer. The latter conjecture has nonetheless still to be tested.

COHERENT CONVECTIVE VORTICAL STRUCTURES

Identification

One way to assess the link between the vortical structures within the mixing layer and the deformation of the zero-mass flux line is to seek for vortex in the class-averaged flowfield. It can be achieved by computing the Q criterion (Hunt *et al.*, 1988) from the class-averaged velocity field $\breve{\mathbf{u}}$. However a difficulty specific to the compressible flow and the reflexion geometry has been encountered: due to the steady strong baroclinic torque located in the region where the incident shock impinges the separated boundary layer, strong Q levels are found in that vicinity for every classes. Several attempts have been made to discard this drawback while not altering the eduction of other structures. Best results have been obtained by subtracting Q values computed from the time-averaged flowfield from Q values obtained for each classes. The results are presented in Figure 6(a) for classes 2 and 9. The residue of the baroclinic vortex is still perceivable but the Q field is dominated by coherent vortical structures with compact supports located within the intervals of X^* corresponding to each class. On the basis of the above results (Fig. 5 and Fig. 6(a)), it is conclude that the coherent vortical structures can be detected using the instantaneous zero mass flux lines.

Characterization

Although the algorithm is able to educe vortical structure, no associated timescale can be directly derived since time information is lost due to the class averaging. It is however of importance to check if the educed structures correspond to the ones whose traces were found by two-points statistics in previous works. Informations related to the timescale of the detected structures can nonetheless be recovered by applying the conditional algorithm to data pre-filtered in time. Because of the clear time-scale separation associated with the SWBLI under consideration (see Dupont *et al.*, 2006, for details), a low-pass filtering with the normalized frequency, *i.e.* Strouhal number $St = fL/U_\infty$, $St \leq 1.65$ allows the removal of the turbulent scales while a

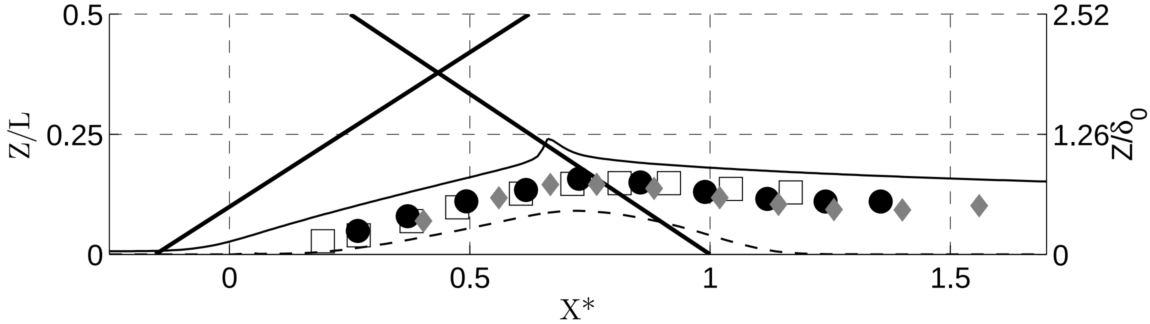

Figure 7. Locations of the Q-weighted barycentre of the structures for all classes educed from data with time shift of -50 , 0 and 50 μs (white, black and gray respectively). See Figure 6 for the other notations in use.

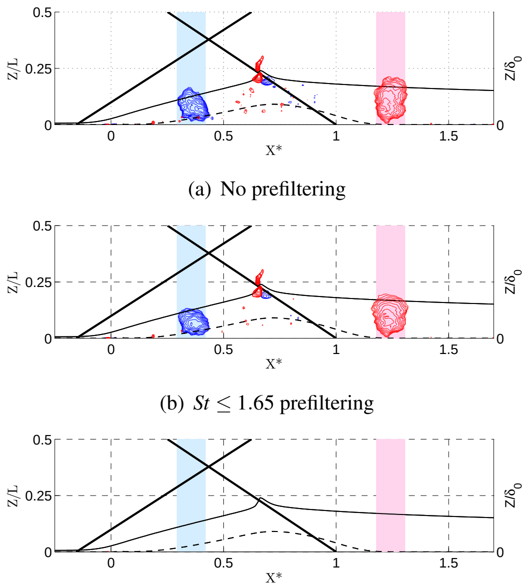

(a) No prefiltering

(b) $St \leq 1.65$ prefiltering

(c) $St \leq 0.1$ prefiltering

Figure 6. Vortical structures educed from the conditionally averaged data by means of the Q criterion for classes 2 and 9 (blue and red respectively). The shock-system location is outlined by the set of thick solid lines. The thin solid line and the dashed one indicate respectively the Mach line and the average zero mass flux lines. The definition of the interval used in conditioning algorithm is also shown.

low-pass filtering with $St \leq 0.1$ preserves the low-frequency unsteadiness only. Structures educed from the $St \leq 1.65$ and $St \leq 0.1$ pre-filtered data are respectively plotted in Figs. 6(b) and 6(c). Comparison of Figs. 6(a), 6(b) and 6(c) demonstrates that the educed vortical structures are associated with the Strouhal number range $[0.1; 1.65]$, in concordance with findings of Dupont *et al.* (2006) and Piponniau *et al.* (2009) for vortices within the mixing layer. Consequently, they are not directly related to both the incoming turbulence and the low frequency unsteadiness.

Another constraint of the original algorithm is that the class averaging is associated with a location rather than a time, as for standard phase averaging. Displacement of the vortical structures can consequently not be tracked directly. The convective nature of the coherent vortical structures can nonetheless be ensured by performing conditional averaging on time-shifted data: for a given time t, the data accumulated to obtain the statistics of the class associated with the location $x_{h^*}(t)$ are taken at time $t-\tau$. The center of the vortical structures is estimated for each class and each time shift by computing the Q-weighted barycentre over the region where Q is positive. The locations of the barycentre computed from time shifts τ equal to -50, 0 and 50 μs are reported in Figure 7 as white boxes, black bullets and gray diamonds, respectively. It is obvious from this figure that the vortical structures are downstream traveling from the mixing layer region up to the shedding region, following trajectories that match well the location of the minima of the mean shear stress.

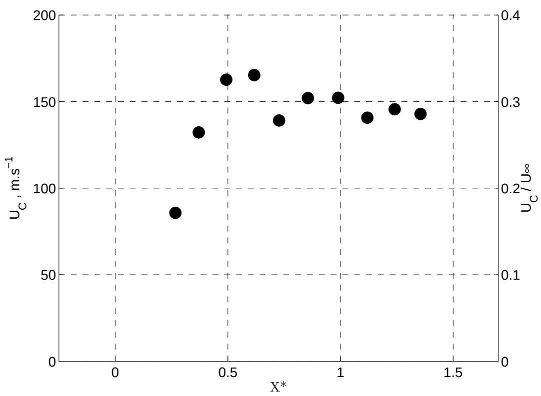

Figure 8. Streamwise convection velocities for each class.

Local estimate of the convection velocity of the structures can also be deduced from the time-shifted data. The streamwise convection velocities are obtained by computing for each class the linear fit of the evolution in τ of the streamwise coordinate of the structure in the least-square sense. Considering time-shifts restricted to $\tau \in [-10\mu s, 10\mu s]$, the linear fits are in very good agreement with the original curves, allowing an accurate estimation of the streamwise velocity. The resulting estimate are plotted in Figure 8. The value obtained using this method are in good concordance with the velocity computed from two-point correlations by Dupont *et al.* (2006), who found streamwise convection velocities around 160 $m.s^{-1}$. Furthermore, in the both cases the convective structure are accelerated in the mixing layer region, while the velocity remains almost constant in the shedding region. The slowing down found at location $x^* \simeq 0.7$ is meaningless since it is a consequence of the imperfect removal of the steady vortex induced in that region by the baroclinic torque. Lastly note that estimations of the vertical convection velocities, typically one order of magnitude lower than their streamwise counterparts, exhibit a low signal-to-noise ratio due to an imperfect statistical convergence despite the long time accumulation of data associated with the LES database under consideration. They are consequently not plotted.

The dimensions of the convective coherent turbulent structures can be derived from the relative velocity fields. One obvious approach would be to consider the extent of the region over which the Q criterion is positive. However values obtained by this method would be overestimated. Since all vortices detected within the interval associated with a given class are averaged irrespectively of their exact location, the resulting class-averaged vortex is smeared over the full width of the conditioning interval. This effect can be neglected only if the vortices are far larger than the conditioning interval. Such prerequisite is not met in the present study, as seen in Figure 6(a), since it would require the use of very small conditioning interval that, in turn, would result in a very poor statistical convergence. One possibility to overcome this problem is to consider a definition similar to the vorticity thickness one. The width W_i and height H_i are respectively computed for class $i = 1 \dots 10$ as:

$$\begin{cases} W_i = \dfrac{\max_x [\hat{w}_i(x, y_{s_i})] - \min_x [\hat{w}_i(x, y_{s_i})]}{\max_x \left[\frac{\partial \hat{w}_i}{\partial x}(x, y_{s_i}) \right]} \\ H_i = \dfrac{\max_y [\hat{u}_i(x_{s_i}, y)] - \min_y [\hat{u}_i(x_{s_i}, y)]}{\max_y \left[\frac{\partial \hat{u}_i}{\partial y}(x_{s_i}, y) \right]} \end{cases} \quad (3)$$

where x_{s_i} and y_{s_i} are respectively the streamwise and wall-normal coordinate of the barycentre above-defined. The results are presented in Figures 9(a) and 9(b) for the width and height, respectively. The width and the height are of the same magnitude. One can observe the similar trend for both dimensions: the structures growth in the beginning of the bubble and their size does not fluctuate much in the shedding region, that is in concordance with Dupont *et al.* (2006) and Cherry *et al.* (1984). The little deflection in the measurements near $0.7X^*$ is probably due to the residue of the baroclinic effect.

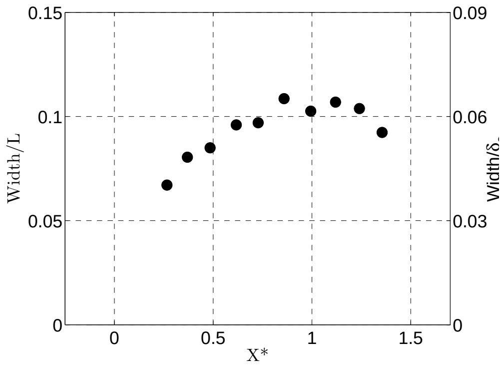

(a) Longitudinal direction

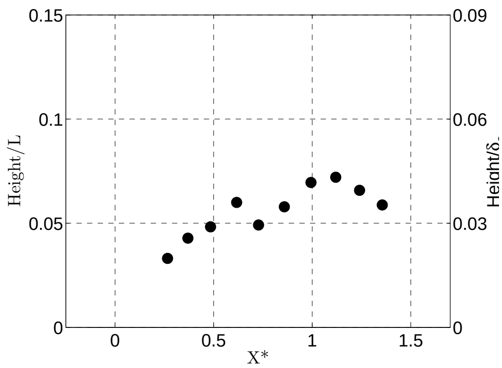

(b) Wall-normal direction

Figure 9. Dimensions of the coherent convective vortical structures.

Wall influence

Since the conditioning algorithm defined in this work can be applied to any quantity and any location, it is possible to study the non-local effect of the convective structures. Signature of the crossing of the structure on wall measurement can for instance be obtained. The class-averaged wall pressure and the skin friction coefficients for classes 2 and 9 are plotted in Figures 10 and 11, respectively. The structures induce the significant localized modulations of C_p and C_f despite the weak amplitude of the celerity fluctuations. One can note that the C_f distribution through the interaction, especially near the reattachment region (red line for class 9), can present some tendancy to the breaking of the bubble into two regions of separated flow with the region of attached flow in between. It can be seen a bit clearer from the Fig. 5. This could be a statistical signature of the instantaneous broken bubble observed by Priebe & Martin (2012) in the direct numerical simulation of a 24° compression ramp in Mach 2.9 flow.

For a given class, the fluctuations of C_p and C_f with respect to the time-averaged mean values typically correspond to 50% to 70% of the local RMS valuse. Consequently wall signature associated with the crossing of the vortical structures would be difficult to discriminate from turbulent fluctuations. It would probably make algorithms only based on wall measurement far less efficient than the one described in this work. Moreover, since the fluctuation are localized in regions varying from class to class with almost no overlapping, the average of these coherent fluctuation over all classes, corresponding to the energy content associated with the convective coherent structures, account for less than 10% of the RMS values. These low levels could explain that methods based on energy-sorting such as POD seems not be able to highlight structures as the one educed using the present algorithm.

CONCLUSION

A new methodology designed to detect and track the coherent structures in shock-boundary layer interaction has been developed and has demonstrated promising results in their statistical characterization. The educed structures are demonstrated to be compact vortical convective structures located in the mixing layer and the shedding region. Their frequency, velocity and trajectory are similar to the ones found in previous works using one- and two-points measurements that were heuristically associated with vortices of the mixing-layer.

Also, as suggested for a long time in subsonic and supersonic separated flows, the development of coherent scales along the mixing layer with size increasing, as well as the

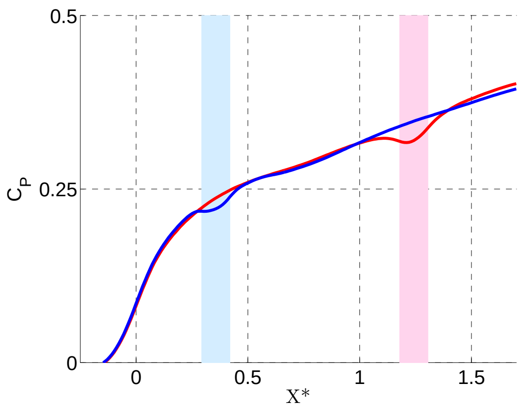

Figure 10. C_p for classes 2 and 9 (blue and red respectively). The definitions of the intervals used in conditioning algorithm are also shown.

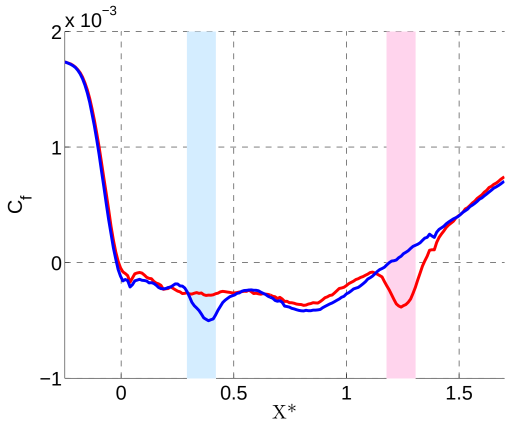

Figure 11. C_f for classes 2 and 9 (blue and red respectively). The definitions of the intervals used in conditioning algorithm are also shown.

shedding process from the second part of the separation region, are validated.

The facts that the above-described algorithm does not required time resolved data and is almost insensitive to the density, at least for the present flow case, make it relevant for the analysis of PIV data.

ACKNOWLEDGEMENT

This work was supported by the French National Agency for Research (ANR) through the DECOMOS project. Computing resources for the LES computation were provided by GENCI-IDRIS under the allocation 2009-021877

REFERENCES

Agostini, L., Larchevêque, L., Dupont, P., Debiève, J.F. & Dussauge, J.P. 2012 Zones of influence and shock motion in a shock boundary layer interaction. *AIAA Journal* **50** (-6), 1377–1387.

Babinsky, H. & Harvey, J.K. 2011 *Shock wave boundary layer interactions*. Cambridge University Press.

Cherry, N. J., Hillier, R. & Latour, M. E. M. 1984 Unsteady measurements in a separated and reattaching flow. *Journal of Fluid Mechanics* **144**, 13–46.

Dupont, P., Haddad, C. & Debiève, J. F. 2006 Space and time organization in a shock induced boundary layer. *Journal of Fluid Mechanics* **559**, 255–277.

Ehrenstein, U. & Gallaire, F. 2008 Global low-frequency oscillations in a separating boundary-layer flow. *Journal of Fluid Mechanics* **614**, 315–327.

Hunt, J. C. R., Wray, A. A. & Moin, P. 1988 Eddies, stream, and convergence zones in turbulent flows. In *Proceedings of the 1988 summer program*, pp. 193–208. CTR, Stanford.

Kiya, M. & Sasaki, K. 1983 Structure of a turbulent separation bubble. *Journal of Fluid Mechanics* **137**, 83–113.

Piponniau, S., Dussauge, J. P., Debiève, J. F. & Dupont, P. 2009 A simple model for low-frequency unsteadiness in shock-induced separation. *Journal of Fluid Mechanics* **629**, 87–108.

Priebe, S. & Martin, M. P. 2012 Low-frequency unsteadiness in shock wave/turbulent boundary layer interaction. *Journal of Fluid Mechanics* p. to be published.